Low-dimensional approximation and control of periodic solutions in spatially extended systems

S. Y. Shvartsman and I. G. Kevrekidis
Department of Chemical Engineering, Princeton University, Princeton, New Jersey 08544
(Received 21 January 1998)

Nonlinear model reduction is combined with numerical continuation and linear state-space control techniques to design regulators for periodic solutions in a spatially extended system. We address issues of construction and systematic evaluation of low-dimensional dynamic models using Galerkin projections on empirical orthogonal eigenfunctions (also known as proper orthogonal decomposition modes or Karhunen-Loève modes). The reduced order dynamical systems are used first to compute the open-loop bifurcation diagrams and then to design feedback controllers stabilizing unstable limit cycles. We outline the steps for discrete-time controller design and computational linear stability analysis of the resulting hybrid (continuous-discrete) closed-loop systems. [S1063-651X(98)14006-0]

PACS number(s): 05.45.+b

I. INTRODUCTION

Periodic trajectories constitute the simplest nontrivial operation mode for continuous, nonstationary processes. Examples from the chemical industry include radio-frequency discharge plasmas [1], reverse flow reactors for pollutant removal [2,3], and temperature swing adsorption units [4]. Associated control problems, such as stabilization and disturbance rejection, are becoming increasingly tractable due to advances in scientific computing and control theory. At this point a lot is known about stabilization of linear time-periodic systems (see, e.g., Ref. [5] and references therein). Problems of regulation of periodic trajectories in nonlinear systems are also being studied using tools of nonlinear control (see, e.g., Refs. [6–8] for recent applications of geometric and H_∞ methods to the control of limit cycles). In the physics community there is a lot of activity in the area of chaos control, where unstable periodic orbits embedded in chaotic attractors are identified and stabilized. Since the 1990 paper by Ott, Grebogi, and Yorke [9], periodic orbits embedded in chaotic attractors have been stabilized in many model and experimental systems (see Ref. [10] for a review). Among the discussed potential applications are novel modes of secure communication, stabilization of nonstationary regimes in lasers, and control of cardiac arrhythmias. The whole journal issues [11,12] dedicated to this subject are representative of the importance of (and activity in) this area.

In this paper we are concerned with the problem of model-based control of limit cycles in dissipative distributed parameter systems, such as chemical reactors. In particular, we address the issue of controller design based on (reduced order) models of the process derived from first principles such as mass, energy, and momentum conservation (as opposed to identified from data–see, e.g., Refs. [13, 14]). Fundamental models usually take the form of evolutionary partial differential equations (PDE's). When discretized, they result in dynamical systems of high order that cannot be easily incorporated into the existing control methodologies. High order and stiffness make even the computing and stability analysis of open-loop periodic solutions in these systems nontrivial. Recent advances in scientific computing, such as approximate inertial manifolds [15], Krylov subspace techniques, and the recursive projection method [16,17], as well as the method of empirical eigenfunctions [18], have been mobilized for this purpose. All of these methods exploit (albeit in diverse ways) the intrinsic time-scale separation of the PDE-derived dynamical systems to approximate their long-term behavior by that of dynamical systems of a (much) smaller dimension. These low-dimensional approximations can usually be associated with dynamics of (slow, ''master'') low-wave-number modes, that are not entirely dominated by dissipative processes, such as diffusion, viscosity, or heat conduction.

Such model order reduction based on time-scale separation has also been successfully employed for control purposes. The basic idea behind this approach is as follows: the controller is based on and designed to address mostly the control-relevant, slow part of the dynamics. The time-scale separation present in the open-loop dynamics (fast decay of ''slave,'' high-wave-number modes), guarantees in many cases the stability of the closed-loop system resulting from such a design [19–22].

In this work, the design of controllers stabilizing open-loop unstable limit cycles is based on low-order dynamical systems generated using the method of empirical eigenfunctions [a.k.a., Karhunen-Loève (KL) or proper orthogonal decomposition (POD)] combined with the Galerkin method. The Karhunen-Loève expansion was previously used to reduce the dimension of the spatially dependent *output* of distributed systems [23], and recently to base control schemes for periodic and quasiperiodic motions on the time-dependent coefficients of the dominant KL modes [24,25]. In our work, this data reduction technique is combined with the PDE to yield accurate dynamical systems used for controller design.

The paper is organized as follows: In Sec. II, we introduce our illustrative example, a nonlinear reaction-diffusion system, exhibiting (stable and unstable) spatiotemporal oscillations. In Sec. III, we briefly review the stabilization problem for a limit cycle, addressing the regulator design based on the original system as well as low order approximations of it. There we introduce formulas for a *particular* controller design—stabilization of a Poincaré map associated with the open-loop periodic orbit. We also derive formulas for evalu-

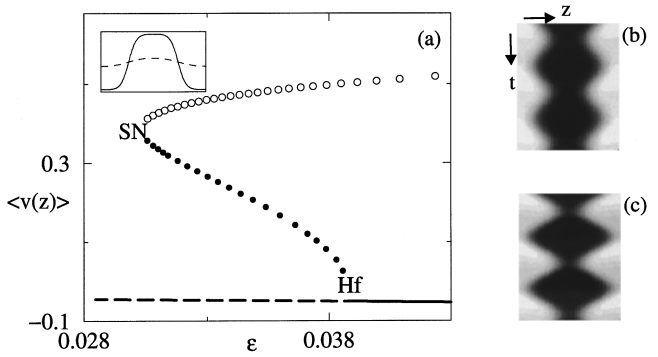

FIG. 1. The open-loop system: (a) Bifurcation diagram for patterned solutions of the type shown in the inset: Solid (broken) lines represent stable (unstable) steady states, while full (empty) circles denote stable (unstable) periodic solutions continued as a function of ϵ for $p_0=-0.03$, $p_1=2.0$, $L=20.0$, and $\delta=2.0$. Hf: Hopf bifurcation point. SN: saddle node of limit cycles. Inset: Nonuniform steady state profile computed for $\epsilon=0.039$; $v(z)[w(z)]$: full [broken] lines, (b) and (c) Representative space-time plots of spatiotemporal limit cycles in (a). Dark (light) corresponds to the high (low) local levels of v. The total time interval is 120 time units. (b) Stable, node-type limit cycle computed for $\epsilon=0.034\,9722\,5$. (c) Saddle-type limit cycle at the same parameter value.

ating *the stability of the closed loop* under such feedback. We then analyze the interconnection of the full system operating in a closed loop with a controller based on a reduced order model. Section V is dedicated to a quick review and evaluation of the model reduction technique (POD-Galerkin method) that we use to obtain our low-dimensional vector fields. In Sec. VI, a computer-assisted study of the closed-loop dynamics and stability of the resulting feedback system is presented, and we conclude in Sec. VII with a discussion and comments motivated by our observations.

II. OPEN-LOOP SYSTEM

The reaction-diffusion system constituting our illustrative example is described by a pair of coupled parabolic partial differential equations with no-flux boundary conditions:

$$v_t=\Delta v+f(v,w)=\Delta v+v-v^3-w, \tag{1}$$

$$w_t=\delta\Delta w+g(v,w)=\delta\Delta w+\epsilon(v-p_1w-p_0), \tag{2}$$

$$v_z|_{0,L}=w_z|_{0,L}=0. \tag{3}$$

In these equations, known as the FitzHugh-Nagumo model [26], v is usually termed the ''activator'' and w the ''inhibitor;'' $\delta=2.0$ is the ratio of diffusivities of the two reacting species, while ϵ represents a ratio of time scales for the kinetic terms; $L=20.0$ is the length of the system box we chose for our study; and $p_1=2.0$ and $p_0=-0.03$ are parameters determining the local dynamics. The PDE has three spatially uniform solutions for these parameter values. The interaction of the nonlinear reaction term with diffusion results in a large number of additional nonuniform steady states. These, for parameter values as in the plot in Fig. 1(a), may take the form of spatial patterns with relatively sharp concentration fronts separating the ignited (up) and extinguished (down) regions of the one-dimensional system. Structured steady states may (and do) lose stability to spatiotemporal dynamics as the system parameters vary. The work of Hagberg and Meron [27] presents the most recent detailed study of stability of frontlike and pulselike solutions in the FitzHugh-Nagumo system.

We illustrate some of the possible transitions by computing the bifurcation diagram associated with a particular patterned (pulselike) solution [the inset in Fig. 1(a)]. In this work we have used a (dealiased) pseudospectral discretization [28] to approximate the reaction-diffusion PDE by a finite size dynamical system. Discretization of each field $[v(z)$ and $w(z)]$ with 31 cosine basis functions resulted in a 62-dimensional system of coupled nonlinear ODE's for the modal amplitudes. This provided a sufficiently converged approximation (the ''full'' model) of the FHN equations for the chosen range of parameters and system size. The branch of stationary solutions in Fig. 1, computed with Newton's method, has the form of an ignited region positioned in the middle of an extinguished domain. Decrease of ϵ below ≈ 0.039 leads to Hopf bifurcation—a pair of eigenvalues of the linearization around this nonuniform steady state crosses the imaginary axis giving rise to oscillations that can be described as periodic changes of the width of the ignited domain (''breathing pulse'' oscillations). This primary bifurcation of the stationary pattern in the system with no-flux boundary conditions was analyzed using singular perturbation methods (with ϵ/δ as a small parameter) in work by Haim *et al.* [29] on breathing spots in a reaction-diffusion system. In this work we are concerned with the analysis and stabilization of unstable oscillatory fronts; these motions arise from a secondary instability (turning point) of breathing fronts upon further decrease of ϵ.

The stable limit cycle that is born at the primary Hopf bifurcation was used to initialize the continuation procedure for the branch of periodic solutions. A shooting method for the computation of limit cycles combined with pseudo-arclength parametrization of the solution branch was used to follow the spatiotemporal oscillations [30]. The evaluation of the overall Jacobian for the Newton's iterations incorporated in the shooting algorithm required a time integration of $N+N^2+N$ (with $N=62$) ODE's for the original dynamical system and the associated variational and parameter sensitivity equations. This time integration was performed using the adaptive step size stiff ODE/sensitivity solver ODESSA [31]. As the amplitude of the breathing front oscillations increases, one Floquet multiplier approaches the unit circle, and the branch of periodic motions turns around at $\epsilon\approx 0.030$ in a saddle-node bifurcation. The saddle-type limit cycles have larger amplitudes and smaller periods than those of corresponding stable ones (and they persist for values of ϵ above the Hopf bifurcation). Our single-shooting code successfully computes saddle-type limit cycles with Floquet multipliers up to 40 ($\epsilon\approx 0.041$).

We will stabilize these unstable (saddle-type) limit cycles through feedback that enters additively into the nonlinear PDE; the feedback is implemented through manipulation of the amplitudes u_j of (l) actuators with spatially nontrivial influence functions $q_j(z)$:

$$v_t=\Delta v+v-v^3-w+\sum_{j=1}^{l}u_jq_j(z), \tag{4}$$

$$w_t = \delta \Delta w + \epsilon(v - p_1 w - p_0). \tag{5}$$

By solving the stabilization problem, we would like to maintain the reaction-diffusion system at its open-loop unstable attractor (spatiotemporal limit cycle) by affecting the eigenstructure of its linearization (Floquet multipliers). The *state* is described by a dynamical system arising from the spectral discretization of this system of PDEs. The input to the system [amplitude(s) of actuator influence function(s) u appearing as parameter(s) in the vector field of this dynamical system] will be manipulated in the closed loop according to the feedback law given by the solution of the stabilization problem.

III. BRIEF REVIEW OF THE STABILIZATION PROBLEM

Full and reduced order systems

We start with nonlinear state-space models

$$\dot{x} = F(x,u), \tag{6}$$

$$\tilde{y} = P(x - \overline{x}), \tag{7}$$

where $x \in \mathbb{R}^n$, $\tilde{y} \in \mathbb{R}^m$, and $u \in \mathbb{R}^l$, and $\overline{x} \in \mathbb{R}^n$ is a constant vector (it provides a convenient reference point in the state space, see below). The matrix P orthogonally projects the difference $(x - \overline{x})$ onto a subspace R_1 of dimension $m \leqslant n$. This subspace of the full state space will be spanned by a (small) number of basis vectors; it is the subspace ''most frequently visited'' by the full system, and it is in this subspace that our low-order model will be constructed. The coordinates of the projection of the state on this subspace are the output assumed available for (and used in) feedback.

Based on our choice of this subspace, we assume that the Galerkin projection of Eq. (6) onto R_1 generates a dynamical system of lower dimension m [reduced order model, (ROM)],

$$\dot{y} = f(y,u), \tag{8}$$

which provides an accurate (in some sense, e.g., *long term*) approximation of the full system dynamics. An example of performing and validating such a procedure is shown in Sec. IV.

Our objective is to stabilize an open-loop $(u=0)$ T-periodic trajectory $x_p(t) = x_p(t+T)$. We approach this by stabilizing the ''corresponding'' periodic trajectory [we assume that it exists and is ''close'' to $\tilde{y} = P(x_p(t) - \overline{x})$] in the reduced order model. The controller for the reduced order model is designed after first deriving a nonlinear discrete-time system by introducing a Poincaré surface (a plane) [32] in R_1. This discrete-time system views the periodic and nearby trajectories at the discrete moments of their (transverse, oriented) intersections with the introduced Poincaré plane. A state-feedback controller for the linearization of this nonlinear system is then designed using conventional linear techniques [33].

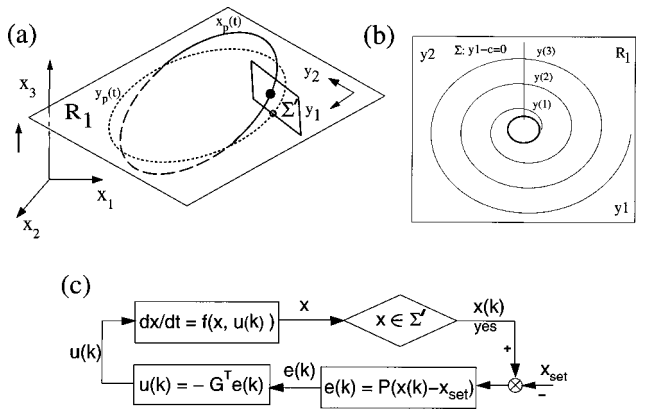

FIG. 2. The stabilization problem: (a) Periodic solution that can be accurately approximated by a low-dimensional model. Bold line—''full'' limit cycle $[x_p(t) = x_p(t+T)]$; thin line—its approximation $y_p(t) = y_p(t+T_0)$ in the low-dimensional subspace R_1. Σ' is the Poincaré plane. (b) Successive iterates of the Poincaré map defined on the plane Σ showing the evolution of perturbations around the approximate limit cycle $y_p(t)$ in the low-dimensional subspace R_1. (c) Closed-loop structure showing the combination of the continuous-time system and the discrete-time controller. The blocks represent the full model, an IF-block for checking the condition of crossing of the Poincaré surface, a comparison with the set point, and a computation of the low-dimensional approximation of the error and the controller.

Analysis of the Poincaré map

Without loss of generality we define our $(m-1)$-dimensional Poincaré plane in R_1 by fixing the first component of the state y of the reduced order model [see Fig. 2(b)]

$$\Sigma : y_1(t) - c = 0. \tag{9}$$

For convenience, we partition the (reduced) state and vector-field vectors (^{T} denotes the vector transpose)

$$y1 = y_1, \quad y2 = (y_2, \ldots, y_m)^T,$$

$$f1 = f_1, \quad f2 = (f_2(y), \ldots, f_m(y))^T.$$

When the ROM governing the evolution of $y(t)$ has a periodic orbit of period $T_0[y_p(t) = y_p(t+T_0)]$ intersecting (transversely) the plane Σ, it is possible to define (locally) an $(m-1)$-dimensional mapping $N(y2(k),u)$ giving the coordinates of the vector $y2(k+1)$ on this plane as a function of its coordinates at the previous intersection with Σ:

$$y2(k+1) = N(y2(k),u) = y2(k) + \int_0^{T(y2(k),u)} f2(y(\tau),u)\, d\tau. \tag{10}$$

The presence of $y2(k)$ and u in the upper limit of the integral denotes the dependence of the ''time of flight'' between successive intersections with Σ on the values of $y2(k)$ and u at the current intersection. This time of flight has to be computed numerically, and we have used Newton's method for this purpose.

The existence of an (open-loop) periodic orbit for the ROM above implies the existence of a fixed point $y2s$ for the map $N(y2,u=0)$,

$$y2s = N(y2s, u=0). \tag{11}$$

According to Floquet theory, the eigenvalues μ of this map linearized around its fixed point (at $u=0$) determine the stability of the (open loop) periodic orbit. When all of these eigenvalues $|\mu|<1$, the fixed point of the map (and the periodic trajectory from which it results) is asymptotically stable. We design a controller that changes the actuator amplitude u when (and only when) the system's trajectory $y(t)$ hits Σ [note the corresponding IF-block in the scheme of the feedback loop shown in Fig. 2(c)]:

$$u(k) = -K(y2(k) - y2s). \tag{12}$$

As the control objective we choose to specify the eigenvalues of the map $N(y2,u(y2))$ linearized around $y2s$ and $u=0$ (our set point).

Linear controller design

The procedure for selection of the matrix of gains $K \in \mathbb{R}^{l\times m-1}$ starts by computing the open-loop linearization. The linearization procedure yields the discrete-time linear system governing the evolution of the error $e(k) \equiv (y2(k) - y2s)$ [note the corresponding block in Fig. 2(c)]:

$$e(k+1) = Ae(k) + Bu(k). \tag{13}$$

The matrices A and B are related to the variational equations determining the sensitivity of the solution at some time t [evaluated on the open-loop limit cycle $y_p(t)$ and $u=0$] to changes in initial conditions $y(t=0)$ and parameter $u(t=0)=u$ values:

$$V(t) \equiv \frac{dy(t)}{dy(t=0)}, \quad \dot{V}(t) = f_y(y)V, \quad V(t=0) = I_{m\times m}, \tag{14}$$

$$S(t) \equiv \frac{dy(t)}{du}, \quad \dot{S}(t) = f_y(y)S + f_u(y), \quad S(t=0) = 0_{m\times l}. \tag{15}$$

We partition the matrices of sensitivities integrated for one period of the open-loop limit cycle (in the ROM) T_0 in the following way:

$$V(T_0) = \begin{pmatrix} V_{11} & V_{12} \\ V_{21} & V_{22} \end{pmatrix}, \quad S(T_0) = \begin{pmatrix} S_1 \\ S_2 \end{pmatrix}, \tag{16}$$

where $V_{11} \equiv [dy1(T_0)]/[dy1(t=0)]$, $S_1 \equiv [dy1(T_0)]/du$ and the other matrix blocks are defined accordingly. Then, linearizing $N(y2(k),u)$, using the Leibniz rule (due to the time-of-flight variation) and the implicit function theorem, we obtain

$$A = V_{22} - f2 \times (V_{12})^T / f1, \tag{17}$$

$$B = S_2 - f2 \times (S_1)^T / f1, \tag{18}$$

where $\times$ denotes the outer vector product. When the discrete time system (A,B) is stabilizable, it is possible to shift the unstable eigenvalues of A inside the unit circle, and stabilize the periodic trajectory applying linear feedback at the moments of its intersection with Σ [33].

Full system in closed loop

We now analyze the stability of the designed controller operating on the full-order vector field [Eq. (6)]. The actuator amplitude will be changed at the intersections of the full system's trajectory $x(t)$ with the plane Σ' [see Fig. 2(a)]:

$$\Sigma' : p_1(x - \overline{x}) = \tilde{y}_1 = c \tag{19}$$

(here p_1 is the first row of the matrix P), and kept constant until the next intersection. Note that the plane Σ introduced in the reduced order model is contained in Σ'. The dynamical system governing the evolution of the state $x(t)$ in-between intersections, with Σ' is given by

$$\dot{x} = F(x, u(k) \equiv -GP(x(k) - x_{\text{set}})), \tag{20}$$

where $G = (0_{l\times 1}, K) \in \mathbb{R}^{l\times m}$ and $x(k), x_{\text{set}}$ are the state vector and the set point at the intersection with Σ'. We see that the closed-loop system trajectory is not smooth at its intersection with Σ', as a result of discontinuous changes in actuator amplitude(s) $u(t)$.

The stability of the closed loop is determined by the evolution of the error vector $(x(k) - x_{\text{set}})$ on Σ'; for this purpose we choose a set of $n-1$ orthogonal coordinate vectors in the subspace orthogonal to p_1^T. The vectors forming a basis for this $(n-1)$-dimensional subspace are provided by QR decomposition of vector $q_1 = p_1^T / \|p_1^T\|$ and stored in the columns of matrix $Q_2 \in R^{n\times n-1}$.

The sensitivity of $x(t)$ to perturbations in initial conditions (on the plane Σ') will be governed by the modified variational equations

$$U(t) \equiv \frac{dx(t)}{dx(t=0)}, \quad \dot{U}(t) = F_x(x_p)U - F_u(x_p)GP,$$
$$U(t=0) = I_{n\times n}. \tag{21}$$

Integrating these equations for a time interval equal to the period (T) of the limit cycle in the full model, we can construct the linearization L of the nonlinear map evolving (in the closed loop), the error between the state vector and the set point on Σ' till the next intersection:

$$L \equiv Q_2^T U(T) Q_2 - Q_2^T F(x_{\text{set}}) \times (q_1^T U(T) Q_2)^T / \langle q_1, F(x_{\text{set}}) \rangle, \tag{22}$$

where $\langle \cdot, \cdot \rangle$ denotes the inner vector product. The closed-loop system is stable when all $n-1$ eigenvalues of L lie inside the unit circle.

IV. MODEL REDUCTION: POD-GALERKIN METHOD

Accurate discretizations of PDE's are traditionally obtained using finite difference, finite element (FEM), or spectral methods. The basis functions for Galerkin projections can either have local support (e.g., FEM) or be global in space (e.g., Fourier modes). The (semiempirical) POD-

Galerkin method uses an alternative set of global basis functions obtained by the principal component analysis of an extensive spatiotemporal data set generated from the time integration of an accurate discretization [34,23]. The basic procedural steps leading to a low-dimensional approximate model include (i) forming a database ensemble of spatiotemporal data, (ii) extracting an empirical eigenfunction basis from the data, and (iii) generating a dynamical system describing the temporal evolution of the modal coefficients of the solution expanded in these basis functions.

The first of these steps is by far the most crucial for the success of the venture: The ensemble is the starting point for forming the finite dimensional subspace (the hyperplane R_1 in Sec. III). All motions orthogonal to this hyperplane will be neglected, and the resulting error is assumed to be small in some sense [34]. The necessity for a large simulational data set, the difficulty in obtaining it, and the lack of rigorous theoretical results concerning convergence properties of the corresponding spectral discretization underscore the empirical nature of the method; on the other hand, it has been very useful in dealing with dynamics and stability analysis of systems beyond the reach of conventional discretizations (see, for example, [18, 35–38]).

The deviations of spatiotemporal data in the ensemble (discretized state $x \in \mathbb{R}^n$) from a convenient reference point, such as the average ($\overline{x} \in \mathbb{R}^n$ in Sec. III) are stored in the ''snapshot matrix'' $MS \in \mathbb{R}^{n \times k}$ [34,23]. The number of columns (k) corresponds to the number of snapshots (instants at which the state of the system has been captured), while the number of rows (n) is equal to the number of ''pixels'' (discretization points, coefficients of Fourier basis functions used in the simulation, etc). The singular value decomposition of the snapshot matrix represents it as a sum of rank 1 matrices

$$MS = \sum_{i=1}^{k} \sigma_i t_i^T \psi_i , \qquad \sigma_1 > \sigma_2 > \cdots > \sigma_k , \tag{23}$$

where σ_i, t_i, and ψ_i represent the singular values and vectors of the snapshot matrix MS.

A high degree of spatiotemporal coherence in the data ensemble will manifest itself in the almost zero magnitude of many of the singular values σ_i, and, consequently, in the fact that a relatively low order ($m \ll n$) truncation of the above summation will provide a good approximation of MS. The set of singular vectors $\{\psi_i\}_{i=1}^m$ forms the basis for a low-dimensional subspace R_1 onto which the higher-dimensional dynamical system (arising from original discretization of a PDE) is projected by the Galerkin procedure.

Some practical comments about the method are in order. There are no *a priori* comprehensive rules for generation of the ensemble from which the empirical basis functions will be extracted. The data should be ''fully representative'' of (i.e., should span) the region of phase space in which it is desired to study temporal evolution or control of the distributed parameter system. For example, if in the closed loop it is desirable to eliminate or restrain motions along particular directions in the phase space, motions along these directions should be included in the ensemble. Since we are interested in a good representation of the dynamics of the closed-loop system, the response to possible actions of the available actuators should be somehow incorporated in the ensemble. Reported ''common sense'' ways of forming a potentially representative ensemble include a combination of spatiotemporal motions at several values of operating parameters [18,35,37], mixing transients from initial conditions distributed randomly around the relevant regions of phase space [39], and storing responses to perturbation of actuators from their nominal settings [38,36,40,41].

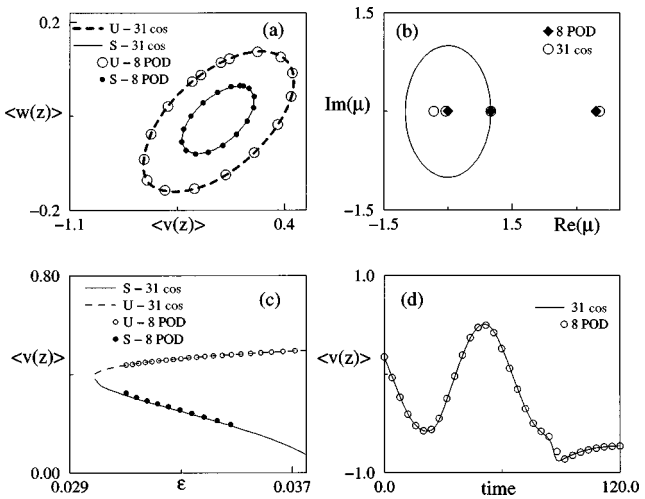

FIG. 3. POD-Galerkin methods: (a) Comparison of the stable and unstable limit cycles computed with 62-dimensional cosine pseudospectral and a 16-dimensional POD-Galerkin discretization at $\epsilon = 0.034\,972\,25$. $U(S)$ denotes unstable (stable) periodic solutions. (b) Leading part of the spectrum (Floquet multipliers) of the unstable periodic solutions in (a) computed with alternative spectral discretizations. (c) Bifurcation diagram of periodic solutions computed with full and reduced order models. (d) Illustration of the short-term tracking capabilities of the 16-dimensional POD-Galerkin vector field: evolution following a perturbation of the saddle-type limit cycle (eventually leading to a distant steady state).

In our implementation this procedure was performed separately for the $v(z)$ and $w(z)$ fields in the FitzHugh-Nagumo PDE. Simulations of the reaction-diffusion system yielded two ensembles [for the $v(z)$ and $w(z)$ fields] that were later SV decomposed to form separate basis sets for spectral discretization. An alternative implementation could have the ''stacked'' profiles $[v(z);w(z)]$ in the ensemble, taking into account in this way the correlation between the two variables. We formed our ensembles in the neighborhood of a periodic motion close to the turning point of the branch of limit cycles in Fig. 1. We combined the transients (including those that lead to distant attractors) at several parameter (ϵ) values with random forcing of the amplitude $u(t)$ of the actuator influence function $q(z)$.

The resulting low-dimensional vector field was required to have attractors (steady states and, especially in this case, limit cycles) close to those of the full system, and to have similar stability and parametric dependence. We evaluated the quality of the approximation by comparing the (open-loop) bifurcation diagrams of attractors of the reduced and full order systems.

For our example, the properties and capabilities of the POD-Galerkin method are illustrated in Fig. 3. The saddle-

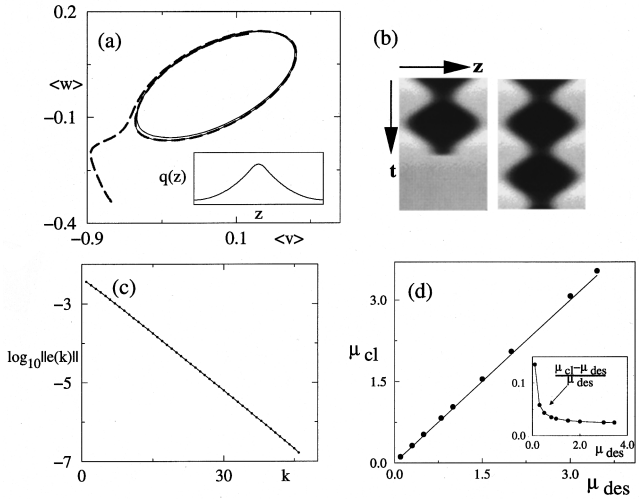

FIG. 4. Closed-loop analysis: (a) Projection (on the plane of the zeroth Fourier modes) of the evolution of the system stabilized by a controller based on the full-order model. Broken (full) lines correspond to open (closed-) loop systems. (a) Inset: spatial form of the actuator influence function $q(z)$ used for controller design based both on full and reduced order models. (b) Space-time plots for transients in (a): left (right)—open (closed) loop. (c) Evolution of the error norm on the Poincaré plane in the linear regime for the closed-loop system. The slope of the curve corresponds to the leading Floquet multiplier specified by controller design. (d) Stabilization using the 16-dimensional POD-Galerkin based model: μ_{cl}—the actual value of the closed-loop Floquet multiplier; μ_{des}—its design value based on the low-order model (see text). (d) Inset: Relative error $[(\mu_{cl}-\mu_{des})/\mu_{des}]$ for the reduced order controller design.

and node-type periodic solutions (coexisting at one parameter value) computed with the full (62-dimensional) and reduced-order (16-dimensional) vector field are shown in Fig. 2(a). The projections of the full and reduced order limit cycles on the plane of zeroth Fourier modes are almost indistinguishable. The periods of reduced order limit cycles are accurate to within 3%. Figure 3(b) demonstrates the ability of the reduced order models to capture the leading part of the spectrum (Floquet multipliers) of the periodic solutions. The accuracy of the approximation is maintained over a wide range of parameter values. This is illustrated by comparing entire branches of periodic solutions in Fig. 3(c). The same low-dimensional vector fields are successful in short-term tracking of off-attractor dynamics. We illustrate this by comparing the transient (from the ''same'' initial conditions) to a distant attractor computed with full and reduced order models in Fig. 3(d).

V. CLOSED-LOOP ANALYSIS

In this section we present the results of the computational dynamic and stability analysis of the closed-loop system with feedback controllers designed on the Poincaré plane. The actuator influence function had the shape shown in the inset of Fig. 4(a). We have chosen it to be symmetric, since the set point and the critical eigenvector (the open-loop unstable limit cycle and the eigenvector of its monodromy matrix corresponding to the largest Floquet multiplier) are symmetric—in this case, they belong to the invariant (under the dynamics of the PDE) subspace of even cosines. We illustrate the performance of controllers, based both on the full (62-dimensional) and reduced (16-dimensional, POD-Galerkin based) order models, in stabilizing the open-loop unstable limit cycle at $\epsilon = 0.034\,97$ (with a leading Floquet multiplier of ≈ 3.538).

The successful closed-loop performance is demonstrated *qualitatively* in Fig. 4(a), showing transient simulations of the full closed-loop model. A point on the limit cycle perturbed (in each component) by 10% from its nominal value was the initial condition for these computations. In the absence of control the system diverged from the limit cycle very quickly. At this level of perturbation rapid evolution into the nonlinear regime was followed by an asymptotic approach to the distant (fully extinguished) steady state [Fig. 4(b), left]. The regulator based on the full order model and designed to place the leading pole of the mapping on the Poincaré plane at 0.8 successfully drove the system to the set-point trajectory [Fig. 4(b), right]. The *quantitative* assessment of the closed-loop stability was done using the formulas derived in Sec. III [Eq. (22)]; the slope of the decay of the error logarithm with successive Poincaré plane intersections was used to double check this calculation [Fig. 4(c)]. The error $\|e(k)\|$ was defined as the 2-norm of the distance of the point on the Poincaré plane from the set point. In the linear regime, the decay rate corresponded very accurately to the eigenvalue at 0.8.

We have also performed transient stability analysis of the closed-loop system under feedback control with regulators designed using the reduced, POD-based models; the full-system unstable limit cycle provides the set point. For a finite range of perturbations of initial conditions and small amplitude disturbances, the controller can keep the system at the open-loop unstable periodic orbit. Using the formulas for stability analysis *with feedback controllers based on reduced order models*, we observed that the closed-loop stability (leading eigenvalue of the mapping on the Poincaré plane chosen for control) is quite close to that stipulated by the reduced order controller design. Figure 4(d) shows the dependence of the actual leading eigenvalue (μ_{cl}) of the closed-loop system (with ROM controller) on the ''nominal'' leading eigenvalue prescribed by ROM-based regulator design (μ_{des}). The relative stabilization error $[(\mu_{cl}-\mu_{des})/\mu_{des}]$ increases as the stability requirements become more stringent. This increase is a consequence of growth of the norm of the matrix of gains G, and is to be expected from general analysis of linear stabilization based on reduced order models [20]. Our set-point periodic orbit and its single unstable eigenvector are symmetric, and so is our actuator function; in fact, the entire open- and closed-loop dynamics possess an invariant subspace (that of even cosines). Symmetries like this can be used to augment the data ensemble [42,43], and the resulting Galerkin projection on POD modes also has corresponding invariant subspaces (spanned by symmetric POD modes). In our case the nonsymmetric modes were stable (had eigenvalues well inside the unit circle); they were not affected by feedback. A nonsymmetric actuator would break these invariant subspaces; a detailed study of symmetry and symmetry breaking due to feedback will be presented elsewhere.

VI. SUMMARY AND DISCUSSION

In this paper we have addressed certain aspects of stabilizing unstable periodic orbits in extended systems (reaction-diffusion PDE's); in particular, we have exploited model reduction for controller design and quantified the stability of the resulting closed-loop systems. Controllers designed to stabilize fixed points of a Poincaré map result in a combination of continuous-time (dynamics between changes in control action) and discrete-time (computation of changes in control action) components. The formulas for closed-loop stability based on this discrete time controller design were obtained from the PDE (and its sensitivities). Such formulas are necessary in the cases when the unstable orbit is *not* ''surrounded'' by a *nearby* attractor, such as a period-doubled or quasiperiodic orbit or a chaotic attractor. The identification step in combined control-identification approaches would fail in these cases, since small perturbations would result in runaway behavior. Low-dimensional models approximating the open- and closed-loop dynamics of accurate spectral discretizations of the PDE were constructed and their explicit parametric dependence exploited for controller design; the good performance of these controllers in the full closed-loop system was explored, and the stability quantitatively documented. This clearly demonstrates the ability of reduced models to capture the (low-dimensional) instability of the open-loop dynamics and the effects of actuation on it. The same controller design and closed-loop analysis can be used for alternative low-dimensional approximations, such as nonlinear Galerkin methods. In our recent work we have used these methods to stabilize patterned steady states in the FHN equations [44].

We end with a brief discussion of alternative approaches and directions. First, the availability of accurate, fully nonlinear, continuous-time low-dimensional models for the dynamics allows one to design more sophisticated (and possibly better) controllers. Computing intersections of the set-point trajectory with several Poincaré planes will result (with obvious modifications of the formulas in Sec. III) in multi-step discrete-time dynamical systems. Controller design for these systems can utilize available techniques for pole-placement [45,46], deadbeat, and linear optimal [47] controllers for linear discrete-time periodic equations. Efficient numerical algorithms for handling such problems (e.g., solving the associated discrete-time periodic Riccati equations [47]) already exist. Control on several Poincaré planes will be beneficial for stabilization of highly unstable periodic orbits (with very large Floquet multipliers). This is completely analogous to the need for multiple shooting algorithms in numerical methods for computing such solutions. Continuous-time feedback control can be thought of as the limiting case of infinitely many control planes. Continuous-time designs of stabilizing controllers (both pole-placement and optimal) can be found in several papers (e.g., Refs. [48–52]). These techniques require one to ''fly'' the differential Riccati equation and/or the linear time-dependent system (both of which require linearization of the nonlinear model around the reference periodic orbit) in the closed loop. Deriving accurate models of *reduced* dimension will clearly make the use of these techniques more viable for dynamical systems of high order, such as discretizations of PDEs. The same holds true for techniques employing time-delayed trajectories for stabilization of unstable orbits [53,54].

Since the controller design for distributed parameter systems is (almost inevitably) based on approximate models, issues of plant-model mismatch are of prime importance for the analysis of the closed-loop stability. We are currently investigating a particular aspect of this mismatch: the effect of using approximate set points (generated by low-dimensional nonlinear Galerkin and POD-based models used for controller design).

The analysis of dynamics of nonlinear distributed parameter systems under feedback control complements the research on open-loop forcing of these systems. Several research groups have reported that open-loop forcing of reacting systems in time and/or space can have ''stabilizing'' effects on the open-loop unstable patterns [55–57]. A combination of the studies of experimental [58–60] and theoretical [61,62] model systems, with the rapidly developing spatially resolving sensing and actuation techniques [63], to harness nontrivial nonlinear behavior in the design and control of nonstationary processes is yet to come.

ACKNOWLEDGMENTS

This research was partially supported through the National Science Foundation and ARPA/ONR. Part of the work was performed when one of the authors was at the ICEHT-FORTH (Patras, Greece) supported by a 94-PENED Grant. We are grateful to Professor Edriss S. Titi for helpful discussions and assistance.

[1] E. Gogolides, H. H. Sawin, and R. A. Brown, Chem. Eng. Sci. **47**, 3839 (1992).
[2] Yu. Sh. Matros and G. A. Bunimovich, Catal. Rev. Sci. Eng. **38**, 1 (1996).
[3] J. Khinast and D. Luss, AIChE. J. **43**, 2034 (1997).
[4] R. T. Yang, *Gas Separation by Adsorption Processes* (Butterworth, Washington, DC, 1987).
[5] S. Bittanti, in *Time Series and Linear Systems*, edited by S. Bittanti, Lecture Notes in Control and Information Sciences Vol. 86 (Springer-Verlag, Berlin, 1986), pp. 141–182.
[6] A. Bacciotti and L. Mazzi, Syst. Control Lett. **24**, 97 (1995).
[7] A. Banaszuk and J. Hauser, Syst. Control Lett. **26**, 95 (1995).
[8] C. C. Chung and J. Hauser, Syst. Control Lett. **30**, 127 (1997).
[9] E. Ott, C. Grebogi, and J. Yorke, Phys. Rev. Lett. **64**, 1196 (1990).
[10] T. Shinbrot, Adv. Phys. **44**, 73 (1995).
[11] IEEE Trans. Circuits Syst. **44**, 10 (1997), special issue on chaos synchronization and control, edited by M. P. Kennedy and M. J. Ogorzalek.
[12] Syst. Control Lett. **31**, 15 (1997), special issue on control of

chaos and synchronization, edited by H. Nijmeijer.
[13] V. Petrov, E. Mihaliuk, S. K. Scott, and K. Showalter, Phys. Rev. E **51**, 3988 (1995).
[14] V. Petrov, S. Metens, P. Borckmans, G. Dewel, and K. Showalter, Phys. Rev. Lett. **75**, 2895 (1995).
[15] M. S. Jolly, I. G. Kevrekidis, and E. S. Titi, Physica D **44**, 38 (1990).
[16] M. F. Schatz, D. Barkley, and H. L. Swinney, Phys. Fluids **7**, 344 (1995).
[17] D. Roose, K. Lust, A. R. Champneys, and A. Spence, Chaos Solitons Fractals **5**, 1913 (1995).
[18] A. E. Deane, I. G. Kevrekidis, G. E. Karniadakis, and S. A. Orszag, Phys. Fluids A **3**, 2337 (1991).
[19] P. V. Kokotovic, H. K. Khalil, and J. O'Reilly, *Singular Perturbation Methods in Control: Analysis and Design* (Academic, New York, 1986).
[20] M. J. Balas, Control Dyn. Syst., 360 (1982).
[21] C.-C. Chen and H.-C. Chang, AIChE. J. **38**, 1461 (1992).
[22] P. D. Christofides and P. Daoutidis, Comput. Chem. Eng. **20**, S1071 (1996).
[23] P. Holmes, J. L. Lumley, and G. Berkooz, *Turbulence, Coherent Structures, Dynamical Systems and Symmetry* (Cambridge University Press, Cambridge, 1996).
[24] S. Chakravarti, M. Marek, and W. H. Ray, Phys. Rev. E **52**, 2407 (1995).
[25] I. Triandaf and I. B. Schwartz, Phys. Rev. E **56**, 204 (1997).
[26] R. FitzHugh, Biophys. J. **2**, 11 (1962).
[27] A. Hagberg and E. Meron, Nonlinearity **7**, 805 (1994).
[28] C. Canuto, M. Y. Hussaini, T. A. Zang, and A. Quarteroni, *Spectral Methods in Fluid Dynamics* (Springer-Verlag, Berlin, 1988).
[29] D. Haim, G. Li, Q. Ouyang, W. D. McCormick, H. L. Swinney, A. Hagberg, and E. Meron, Phys. Rev. Lett. **77**, 190 (1996).
[30] M. Kubicek and M. Marek, *Computational Methods in Bifurcation Theory and Dissipative Structures* (Springer-Verlag, Berlin, 1983).
[31] J. R. Leis and M. A. Kramer, ACM Trans. Math. Softw. **31**, 61 (1988).
[32] J. Guckenheimer and P. Holmes, *Nonlinear Oscillations, Dynamical Systems and Bifurcations of Vector Fields* (Springer-Verlag, New York, 1983).
[33] K. Ogata, *Discrete-Time Control Systems* (Prentice-Hall, Englewood Cliffs, NJ, 1995).
[34] L. Sirovich and J. D. Rodriguez, Phys. Lett. A **120**, 211 (1987).
[35] A. K. Bangia, P. F. Batcho, I. G. Kevrekidis, and G. Em. Karniadakis, SIAM J. Sci. Stat. Comput. **18**, 775 (1997).
[36] A. Theodoropoulou, R. A. Adomaitis, and E. Zafiriou, IEEE Trans. Semicond. Manuf. **11**(1), 85 (1998).
[37] R. A. Sahan, A. Liakopoulos, and H. Gunes, Phys. Fluids **9**, 551 (1997).
[38] H. Aling, S. Banerjee, A. K. Bangia, V. Cole, J. L. Ebert, A. Emami-Naeini, K. F. Jensen, I. G. Kevrekidis, and S. Shvartsman (unpublished).
[39] M. D. Graham and I. G. Kevrekidis, Comput. Chem. Eng. **20**, 495 (1996).
[40] H. M. Park and D. H. Cho, Chem. Eng. Sci. **51**, 81 (1996).
[41] H. P. Loffler and W. Marquardt (unpublished).
[42] L. Sirovich, Quart. Appl. Math. **45**, 583 (1987).
[43] G. Berkooz and E. S. Titi, Phys. Lett. A **174**, 94 (1993).
[44] S. Y. Shvartsman and I. G. Kevrekidis, AIChE (to be published).
[45] M. Kono, Int. J. Control **32**, 149 (1980).
[46] P. T. Kabamba, IEEE Trans. Autom. Control. **31**, 1950 (1986).
[47] J. J. Hench and A. J. Laub, IEEE Trans. Autom. Control. **39**, 1197 (1994).
[48] R. A. Calico and W. E. Wiesel, J. Guid. Control Dyn. **7**, 671 (1984).
[49] W. E. Wiesel, Phys. Rev. E **49**, 1990 (1994).
[50] W. E. Wiesel, J. Guid. Control. Dyn. **18**, 995 (1995).
[51] A. Tornambe and P. Valigi, Syst. Control Lett. **28**, 189 (1996).
[52] M. J. Balas and Y. J. Lee, in Proceedings of the American Control Conference, Albuquerque, NM, 1997 (unpublished), pp. 2667-2671.
[53] K. Pyragas, Phys. Lett. A **170**, 421 (1992).
[54] M. E. Bleich, D. Hochheizer, J. Moloney, and J. E. S. Socolar, Phys. Rev. E **55**, 2119 (1997).
[55] M. Baer, A. K. Bangia, I. G. Kevrekidis, G. Haas, H.-H. Rotermund, and G. Ertl, J. Phys. Chem. **100**, 19 106 (1996).
[56] A. Hagberg, E. Meron, I. Rubinstein, and B. Zaltzman, Phys. Rev. Lett. **76**, 427 (1996).
[57] R.-M. Mantel and D. Barkley, Phys. Rev. E **54**, 4791 (1996).
[58] V. Petrov, Q. Ouyang, and H. L. Swinney, Nature (London) **388**, 655 (1997).
[59] S. Mironov, M. Vinson, S. Mulvey, and A. Pertsov, J. Phys. Chem. **100**, 1975 (1996).
[60] A. P. Munuzuri and M. Markus, Phys. Rev. E **55**, R33 (1997).
[61] R. Martin, A. J. Scroggie, G.-L. Oppo, and W. J. Firth, Phys. Rev. Lett. **77**, 4007 (1996).
[62] V. S. Zykov, A. S. Mikhailov, and S. C. Mueller, Phys. Rev. Lett. **78**, 3398 (1997).
[63] H.-H. Rotermund, K. Krisher, and B. Pettinger, in *Frontiers of Elechtrochemistry, Vol. IV: Imaging of Surfaces and Interfaces*, edited by J. Lipkowski and P. N. Ross (VCH, New York, 1997).